ADVANCED ROBOTICS, 2017
VOL. 31, NO. 8, 441–452
http://dx.doi.org/10.1080/01691864.2016.1273135

FULL PAPER

Stability and joint stiffness analysis of legged robot's periodic motion driven by McKibben pneumatic actuator

Yasuhiro Sugimoto, Daisuke Nakanishi, Motoki Nakanishi and Koichi Osuka

Department of Mechanical Engineering, Osaka University, Suita, Japan

ABSTRACT

A McKibben-type pneumatic actuator is widely used as a convenient actuator for a robot with a simple actuator model and a simple control method. However, the effect of its characteristics on the stability of robot motion has not been sufficiently discussed. The purpose of our research is to analyze the influence that the various characteristics of a McKibben pneumatic actuator has on the stability of movements generated by the actuator. In this study, we focus on a periodic motion, which is one of the common movements of robots. We introduce a stability criterion for periodic motion similar to our previous work, in which stability of musculo-skeletal system was discussed, and show that the criterion is always satisfied. Next, we focus on a redundancy of air pressure inputs. As one of application of the redundancy, we investigate the joint stiffness of a robot and propose a design procedure of inputs based on a reference period trajectory and the desired joint stiffness. The stability analysis and design of joint stiffness are verified not only through numerical simulations but also through experiments with a developed 1-DOF legged robot.

ARTICLE HISTORY
Received 22 June 2016
Revised 19 October 2016
Accepted 5 December 2016

KEYWORDS
McKibben-type pneumatic actuator; stability analysis; periodic motion; joint stiffness analysis

1. Introduction

In research on robotics, a McKibben pneumatic actuator (MPA), which is a type of soft actuator, has received considerable attention. This actuator has mechanical compliance and exhibits many good characteristics; it is very light, has a high force-to-weight ratio compared with other types of actuators, and it can flexibly comply with outside forces. Because of these above-mentioned properties, MPAs have been employed in various robots, and robots actuated by MPAs can achieve comparatively stable motions [1–5]. Remarkably, these studies accomplished various dynamic robot motions such as walking and jumping only with a simple control based on a rule of thumb, or even with less complicated control and/or control that depends on simple modeling. However, the important features of the actuator and the manner in which they influence stable robot motion have yet to be adequately discussed. To promote the research and application of an MPA, it is necessary to investigate whether the MPA's own characteristics can contribute to the realization of stable robot movements and whether such a contribution can be achieved via an interaction with a mechanical structure of a robot and the MPA.

Therefore, we proposed a relatively simple MPA model and analyzed the stability of the stationary posture [6,7]. In the study, we derived a stability condition analytically and verified whether the condition was satisfied based on the property of the MPA and the interaction with the properties of the actuator and the mechanical structure of the robot. Here, we extend our previous study to a *periodic motion* driven by an MPA. Periodic motion is a common dynamic movement of a robot. Previous robots actuated by pneumatic artificial muscles could realize various dynamic periodic motions, such as walking [2,3,5], continuous jumping [8,9] and running [10,11]. And hence, it is worth considering this motion in our study. We derive a stability criterion for periodic motion and show that the derived criterion is always satisfied.

Next, we focus on a redundancy of air pressure inputs. As one of application of the redundancy, we investigate the joint stiffness of a robot. The joint stiffness of the robot is also an important property. Furthermore, the joint stiffness regulation will offer an energy storing property or protection against high disturbance forces [12]. These properties are essential to realize more dynamic robot movement. Hence, it is also worth investigating this property combining the stability analysis of periodic motions. We analyze the joint stiffness and discuss the relationship among the joint stiffness, the reference period trajectory and pressure inputs. Using the derived relationship, we propose a design procedure of inputs based on a reference period trajectory and the desired joint stiffness. Because of it's compliant property of

CONTACT Yasuhiro Sugimoto yas@mech.eng.osaka-u.ac.jp

pneumatic artificial muscles including MPA, applications and control strategies of joint stiffness of robots actuated by pneumatic artificial muscles have been already investigated [12–15]. The difference between our proposed method and previous works is that the proposed design procedure of inputs is based on the stability analysis of periodic motions and then it can realize both a desired joint stiffness and reference period trajectory simultaneously under the stability condition.

This paper consists of five sections. After the introduction in this first section, Section 2 describes the details of model of MPA and a legged robot. Section 3 describes the stability criteria for periodic motions and the result of the stability analysis are verified through numerical simulations and validation experiments. In Section 4, the joint stiffness of a robot is investigated. Depending on the analysis of the joint stiffness and result of Section 3, a design procedure of inputs based on a reference period trajectory and the desired joint stiffness are proposed. The stability analysis and design of joint stiffness are verified not only through numerical simulations but also through experiments. Finally, Section 5 presents the conclusion.

2. Model of MPA and legged robot

2.1. Model of MPA

An example of an MPA is shown in Figure 1. The MPA mainly consists of two components: a silicon rubber tube and a mesh of nylon fibers. The mesh of nylon fibers surrounds the silicon rubber tube (Figure 1(b)). Actuation is achieved by supplying a compressed air into the bladder of the rubber tube. The compressed air expands the bladder whose volume expands. As the volume of the inner bladder increases, the mesh of the nylon fibers becomes shorter because it cannot be extended laterally (Figure 1(a)). From this mechanism, the MPA produces tension and becomes 'an actuator'.

Much research has also been carried out on the property evaluation and detailed modeling of the MPA [16–21]. Such attempts have been successful to some extent and detailed models of MPAs have already been proposed. However, a complicated model, in which the various detailed characteristics of the actuator elucidated by a previous work are considered, is potentially too complex and makes it difficult to understand the characteristic of the MPA that contributes to movement stability.

In our previous study [6], we proposed a relatively simple MPA model for the stability analysis of robot motions generated by the MPA. In this model, the actuator force f_s consists of a force, which is derived from air pressure, and a force derived from the elasticity of the MPA as follows:

$$f_s(P',\ L) = -P'\frac{\mathrm{d}V_b}{\mathrm{d}L} + V_r\frac{\mathrm{d}W}{\mathrm{d}L} \tag{1}$$

where P' is the relative pressure between the absolute internal air pressure and the environment pressure. L is the length of the MPA. V_r is the volume occupied by the bladder and calculated using the radius, length, and bladder thickness of the actuator. V_b is the actuator's interior volume and calculated using the radius and length. And, W is the strain energy density function. The details of this model are described in the Appendix. The model may seem slightly complicated, but the only variables in this model are P' and L; the other parameters are fixed. This makes it easy to analyze motions of the robot driven by the MPA. Further, it was verified through validation experiments that this model can express the MPA properties relatively well.

The force f_s in Equation (1) is independent of the contractile velocity of the actuator v. Because silicon rubber, which is used in MPA, has viscoelastic characteristics, the MPA model should have a velocity-dependent property. Then, we suppose a series contractile velocity-dependent term $f_v(v)$ as:

$$f(P',\ L,\ v) = -P'\frac{\mathrm{d}V_b}{\mathrm{d}L} + V_r\frac{\mathrm{d}W}{\mathrm{d}L} - f_v(v). \tag{2}$$

Although a detailed formulation of $f_v(v)$ has not yet been achieved, it was experimentally verified that the actuator force decreases in the direction of the actuator contractile velocity v, that is, the differentiation of the actuator force f with respect to the actuator contractile velocity v becomes negative

$$\frac{\mathrm{d}f}{\mathrm{d}v} < 0 \tag{3}$$

in our previous work [6]. And also in [6], the force almost linearly decreased with the contraction velocity. From the experimental result, as a most simple model, we assume the term $f_v(v)$ as the following:

$$f_v(v) = \gamma v \quad (\gamma > 0). \tag{4}$$

Using this MPA model, we analyze the stability and design pressure inputs for a periodic motion of legged robot driven by the MPA.

2.2. Model of legged robot

Figure 2 shows a legged robot model that is used in this study. In this model, an antagonistic pair of MPAs is arranged around the knee. Only bending and stretching

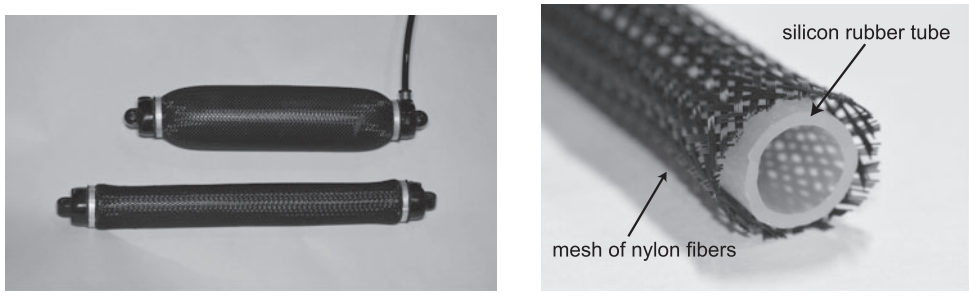

(a) MPA is contracted when air is supplied (upper), and is relaxed when air is expelled (bottom).

(b) Cross section of MPA.The mesh of nylon fibers surrounds the silicon rubber tube.

Figure 1. An example of McKibben-type pneumatic actuator.

movements in a perpendicular direction can be achieved by bending the knee. To simplify the following discussion, the motion of the representative mass of the leg and hip (m in Figure 2) is assumed to be constrained in a vertical one-dimensional movement, that is, the hip does not move horizontally. Definitions of each symbol and values in the figure are shown in the Appendix.

The geometric transformation between the ground reaction force F and extensor and flexor actuator forces f_e and f_f for vertical movements can be described as follows:

$$F(X, V, P'_e, P'_f) = G_e(X) f_e(P'_e, L_e, v_e) - G_f(X) f_f(P'_f, L_f, v_f) \quad (5)$$

$$f_e(P'_e, L_e, v_e) = -P'_e \frac{\mathrm{d}V_{be}}{\mathrm{d}L_e} + V_r \frac{\mathrm{d}W_e}{\mathrm{d}L_e} - \gamma_e v_e \quad (6)$$

$$f_f(P'_f, L_f, v_f) = -P'_f \frac{\mathrm{d}V_{bf}}{\mathrm{d}L_f} + V_r \frac{\mathrm{d}W_f}{\mathrm{d}L_f} - \gamma_f v_f \quad (7)$$

where X is the vertical displacement of the hip from the ground. L_e and L_f are the length of the extensor (outside) and the flexor (inside) MPA, respectively, v_e and v_f are the actuator contractile velocity of the extensor and the flexor MPA respectively; and P'_e and P'_f are the air pressure of the actuator that acting as an extensor and as a flexor, respectively.

Geometric functions $G_e(X)$ and $G_f(X)$ in Equation (5) can be derived from the equilibrium of the moment of the robot as follows:

$$G_e(X) = \frac{r}{L_o L_u \sin\beta} X, \; G_f(X) = \frac{L_1 L_2}{L_o L_u l_{Mf}} X \quad (8)$$

where β and l_{Mf} can be derived geometrically as follows:

$$\beta(X) = \cos^{-1}\left(\frac{L_o^2 + L_u^2 - X^2}{2L_o L_u}\right) \quad (9)$$

$$l_{Mf}(X) = \sqrt{L_1^2 + L_2^2 - 2L_1 L_2 \cos\beta(X)}. \quad (10)$$

L_e, L_f, v_e and v_f can be written as

$$L_e(X) = L_{e0} - r(\beta(X) - \beta_0) \quad (11)$$

$$L_f(X) = L_{f0} + l_{Mf}(X) - l_{Mf0} \quad (12)$$

$$v_e(X, V) = G_e(X) V \quad (13)$$

$$v_f(X, V) = -G_f(X) V \quad (14)$$

where $V = \dot{X}$, L_{e0} and L_{f0} are the initial length of the extensor and flexor MPAs, β_0 is the initial angle of the knee and l_{Mf0} is the sum of the initial flexor MPA length and wire length.

The dynamical equation of the system can be written as follows:

$$\frac{\mathrm{d}}{\mathrm{d}t}\begin{pmatrix} X \\ V \end{pmatrix} = \begin{pmatrix} V \\ F/m - g \end{pmatrix}. \quad (15)$$

In this study, we assume that the air pressures of MPA P'_e, P'_f can be regulated arbitrarily under $P'_e \geq 0$ and $P'_f \geq 0$. Consequently, the inputs of the system (15) are the air pressures of the MPA P'_e, P'_f.

Substituting Equations (5)–(7) into Equation (15), the air pressure of the extensor actuator P'_e for a provided reference trajectory $(\hat{X}, \hat{V})$ can be calculated as

$$P'_e(\hat{X}, \hat{V}, P'_f) = \frac{1}{\mathrm{d}V_{be}/\mathrm{d}L_e}\left[V_r \frac{\mathrm{d}W_e}{\mathrm{d}L_e} - \gamma_e v_e - \frac{1}{G_e}\left\{m\dot{\hat{V}} + mg + G_f\left(-P'_f \frac{\mathrm{d}V_{bf}}{\mathrm{d}L_f} + V_r \frac{\mathrm{d}W_f}{\mathrm{d}L_f} - \gamma_f v_f\right)\right\}\right]. \quad (16)$$

Using Equation (16), P'_e can be calculated uniquely from P'_f. This implies that inputs P'_f and P'_e are independent on the state (X, V), that is, P'_f and P'_e are feedforward inputs. This relation also implies that there is a redundancy in the selection of P'_f and P'_e to achieve the

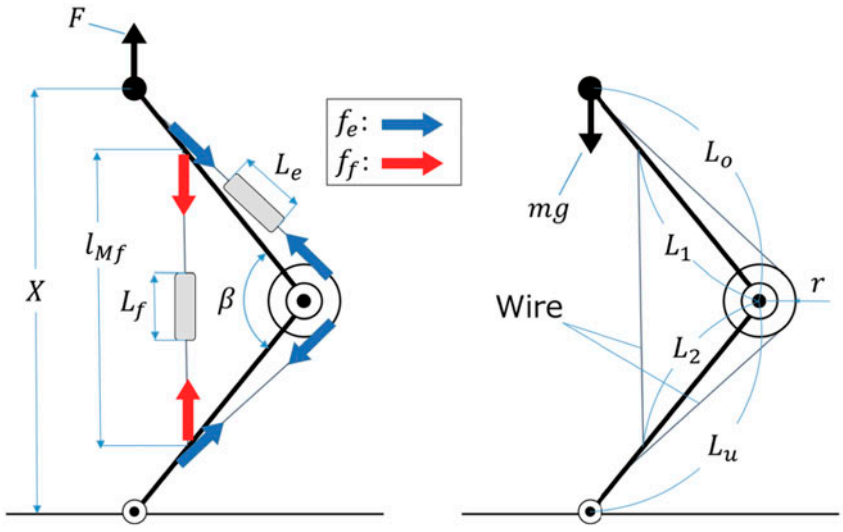

Figure 2. Parameters and constants of the robot model.

provided $(\hat{X}, \hat{V})$. The analysis of this redundancy will be described in Section 4.

3. Analysis of stability of periodic motion

3.1. Stability criterion for periodic motion

In this section, we analyze the stability of the periodic motion of the legged robot shown in Figure 2. In this paper, the stability of the periodic motion is defined as 'orbitally stability' and the stability is determined based on Poincaré map or Floquet theory.

By linearizing the system of Equation (15), the following linear system can be derived;

$$\frac{\mathrm{d}}{\mathrm{d}t}\begin{pmatrix}\tilde{X}\\ \tilde{V}\end{pmatrix} = \begin{pmatrix}0 & 1\\ a_2 & a_1\end{pmatrix}\begin{pmatrix}\tilde{X}\\ \tilde{V}\end{pmatrix} \tag{17}$$

where $\tilde{X} = X - \hat{X}$, $\tilde{V} = V - \hat{V}$ and

$$a_1 = \frac{1}{m}\frac{\partial}{\partial V}(G_e f_e - G_f f_f), \quad a_2 = \frac{1}{m}\frac{\partial}{\partial X}(G_e f_e - G_f f_f) \tag{18}$$

The stability criterion for the periodic motion can be given by the following theorem.

Theorem 1: *System (17) becomes stable for periodic motions whose period is T if and only if:*

$$\int_0^T a_1(t)\mathrm{d}t < 0 \tag{19}$$

***Proof*:** This criterion can be derived in the same manner as derived in the previous work [22], in which the stability of the periodic motion for a **musculo-skeletal** system was discussed. Except for the model of force f_e and f_f (muscle or MPA), the musculoskeletal system in [22] and the legged robot (Figure 2) basically have the same structure. □

Using this theorem, we analyze the stability of the periodic motion driven by the MPA.

From Equations (13), (14) and (4), a_1 in Equation (18) can be transformed to

$$\begin{aligned} a_1 &= \frac{1}{m}\frac{\partial}{\partial V}(G_e f_e - G_f f_f)\\ &= \frac{1}{m}\left(G_e \frac{\partial v_e}{\partial V}\frac{\partial f_e}{\partial v_e} - G_f \frac{\partial v_f}{\partial V}\frac{\partial f_f}{\partial v_f}\right)\\ &= \frac{1}{m}\left(G_e^2 \frac{\partial f_e}{\partial v_e} + G_f^2 \frac{\partial f_f}{\partial v_f}\right)\\ &= -\frac{1}{m}(G_e^2\gamma_e + G_f^2\gamma_f). \end{aligned} \tag{20}$$

From the definition of f_v (Equation (4)), $\gamma_e > 0$ and $\gamma_f > 0$. Therefore, a_1 always has a negative value; hence, the stability criterion in Theorem 1 is always satisfied similar to the musculo-skeletal system discussed in [22] although there is a slight difference in the structure of the knee. From these facts, it can be said that the periodic motion of the system (17) is locally always stable.

In this investigation, the property of the MPA, especially the force-contractile velocity property f_v plays a significant role. However, to verify the criterion, it is not necessary to define a concrete form of f_v. A sufficient condition can be derived only with the inequality (3), which describes one of the interesting properties of the MPA. To design various inputs P_f' and P_e' in the following section, we formulated f_v as Equation (4).

Remark 1: Although the above discussions are valid for any periodic motions mathematically, this discussion does not make sense unless the period motion is feasible, that is, there exist appropriate actuator inputs that can achieve the periodic motion.

3.2. Simulation

In this section, we verify the result of the stability analysis from the previous section via some numerical simulations.

In this study, we set a reference periodic trajectory $(\hat{X}, \hat{V})$ as a following simple harmonic oscillation:

$$\begin{pmatrix} \hat{X} \\ \hat{V} \end{pmatrix} = \begin{pmatrix} \hat{X}_0 + \hat{A}\sin\omega t \\ \hat{A}\omega\cos\omega t \end{pmatrix} \tag{21}$$

where $\hat{A}$ and $\omega(\ = 2\pi/T)$ are the amplitude and frequency of oscillation and $\hat{X}_0$ is the center of oscillation.

First, we set P'_f as constant (= 0.5 bar) and $\hat{X}_0 = 0.8$ m, $\hat{A} = 0.02$ m and $T = 3$ s. These parameters were chosen as an example of feasible and relatively large periodic motion. P'_e is calculated based on these parameters and Equation (16) and shown in Figure 3.

Figure 4 shows the simulation results with the calculated air pressures P'_e and P'_f in Figure 3. The parameters of the robot model used in the simulation are listed in the Appendix. To examine the robustness of the system, we added the initial state error ($X_0 - \hat{X}_0 = 0.02$ m and $V_0 - \hat{V}_0 = 0.1\,\mathrm{m\,s^{-1}}$]) or a disturbance after convergence on periodic motion. As the disturbance, we added a 20 N force for 0.05 s to the mass of robot. The results with the initial state error and with the disturbance are shown in Figure 4(a) and (b), respectively. In both cases, the state X converged to the given periodic trajectory $\hat{X}$ after a certain period of time. Next, to investigate the effect of modeling error, we changed $\gamma(\ = \gamma_e = \gamma_f)$ or m in the simulation model though P'_f and P'_e were designed based on nominal values $\gamma_0 = 30$ Ns/m or $m_0 = 3.754$ kg. Figure 4(c) and (d) shows the simulation results respectively when small initial state error $X_0 - \hat{X}_0 = 0.01$ m was also added. Figure 4(c) shows that the trajectory of X converged to almost same trajectory with reference trajectory when γ was changed. Figure 4(d) shows the results when m was changed. In this case, the trajectory of X converged to stable periodic motions regardless of the initial state error although the trajectory of X has some steady-state error derived from the modeling error. From this result, it is verified that the periodic motion of a legged robot system from Equation (15) driven by the MPA model from Equation (2) becomes stable as analyzed in Section 3.1.

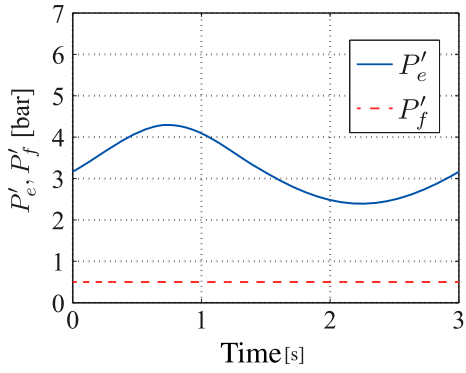

Figure 3. Designed inputs P'_e with $P'_f = 0.5$ bar.

3.3. Experiment validation

Next, we confirmed the stability analysis through experiments with a real machine. Figure 5(a) shows an experimental device that we developed based on the robot model in Figure 2. The upper and lower links consist of two aluminum frames and shafts sandwiched in between frames. An ankle and a knee can rotate around the shaft. To achieve the vertical one-dimensional movement of the hip, a lumbar part is smoothly constrained with a linear sliding bushing (Figure 5(b)). A knee part consists of a pulley. The values listed in the Appendix, which were used in the simulation, were derived from the parameters of the developed robot. The experimental setup is shown in Figure 6. The pressure of compressed air was regulated from the PC through electromagnetic regulators. The state of the robot (X, V) could be obtained from a rotary encoder which was attached at the lumbar part.

Figure 7(a) shows an experimental result with P'_e and P'_f in Figure 3 after convergence on periodic motion. The initial state was set as $(X_0, V_0) = (0.8\,\mathrm{m}, 0)$. In addition, we also set P'_f as $P'_f = 1 - 1\sin\omega t$ bar and calculated P'_e in the same manner. The result is shown in Figure 7(b). To investigate the response to the disturbance, we also conducted other experiment. In this experiment, same P'_f and P'_e in Figure 3 were used and we provided an impulsive force to the lumbar part of the robot around $t = 3.0$ s, $t = 9.0$ s and $t = 15.0$ s as a disturbance. Figure 7(c) shows the experimental results. It can be seen that the trajectory of X was disturbed by the impact but it converged to the reference trajectory soon. The robot showed a stable periodic motion and the desired trajectory was almost achieved only by feedforward inputs P'_e and P'_f. Although there were some tracking errors and delays, it will be possible to reduce them by improving the MPA model or by feedback control. An appropriate controller design which corresponds to the stability analysis is left as a future work.

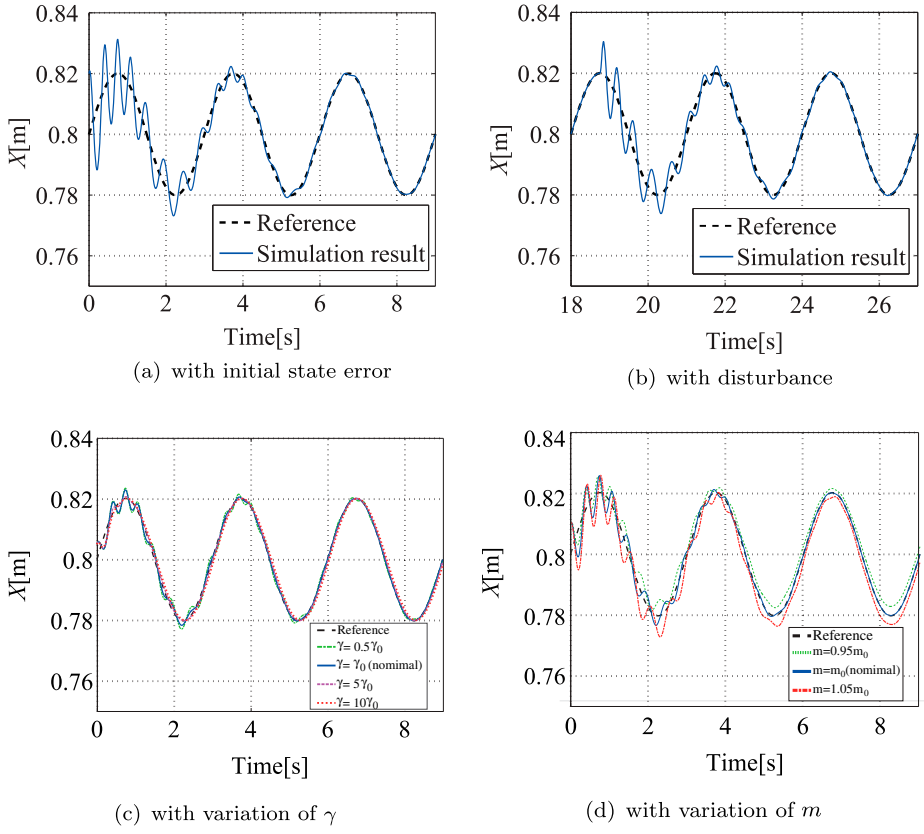

(a) with initial state error (b) with disturbance

(c) with variation of γ (d) with variation of m

Figure 4. Simulation results.

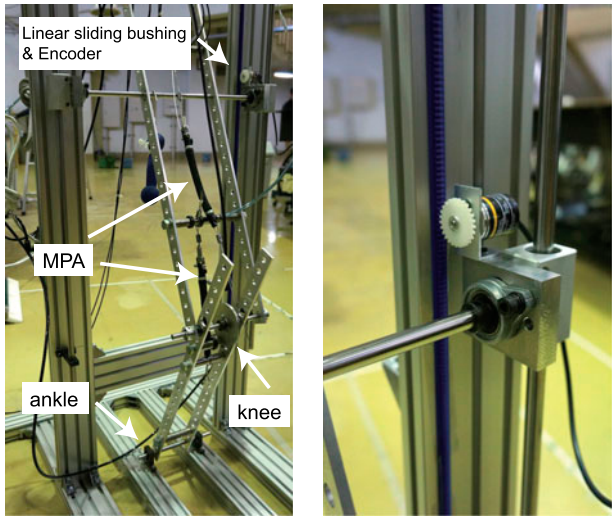

(a) Overview (b) Linear sliding bushing

Figure 5. 1-DOF legged robot driven by MPA.

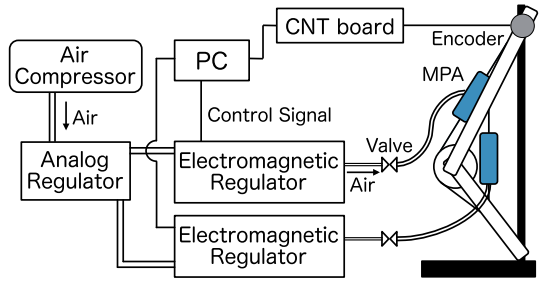

Figure 6. Schematic of experimental setup.

4. Inputs design based on reference periodic motion and desired joint stiffness

The stability analysis in Section 3 argues that any P'_f and P'_e values which realize a periodic motion of the system (17) can always realize a locally stable periodic motion. Based on the strong guarantee of stability, we can focus on the design of various inputs without paying attention to the stability. Furthermore, as described in Section 2.2, there is redundancy in the selection of P'_f and P'_e which can achieve $(\hat{X}, \hat{V})$. Here, we investigate the application of the redundancy. In this study, we focus on the joint stiffness and design some input patterns based on the analysis of the joint stiffness.

4.1. Various air pressure inputs P'_f and P'_e

To simplify the design of inputs P'_f and P'_e, we adopt the following function for P'_f:

$$P'_f = P'_{f0} + A_f \sin \omega t \tag{22}$$

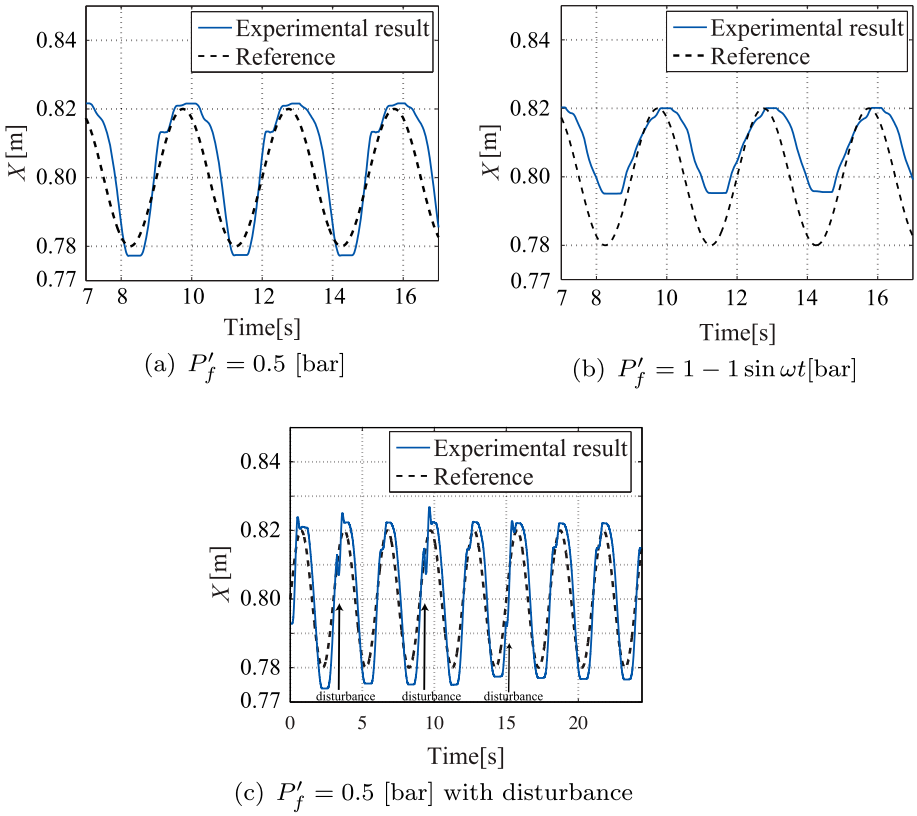

(a) $P'_f = 0.5$ [bar] (b) $P'_f = 1 - 1\sin\omega t$[bar]

(c) $P'_f = 0.5$ [bar] with disturbance

Figure 7. Experimental results to investigate the effect of various P'_f or disturbance.

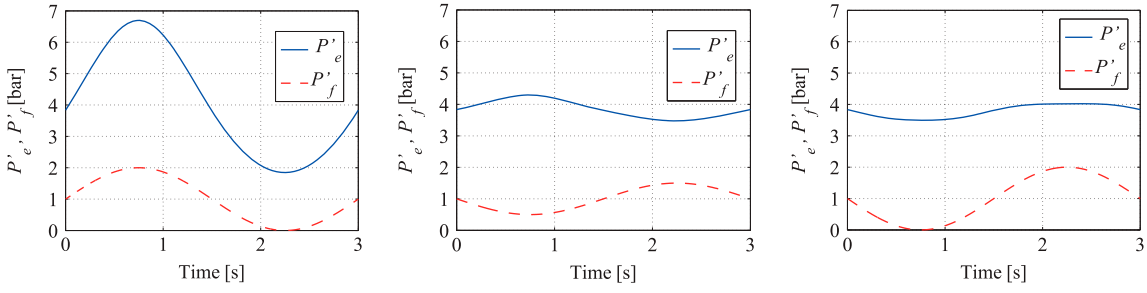

(a) Mode 1 $(P'_f = 1 + 1\sin\omega t$[bar]) (b) Mode 2 $(P'_f = 1 - 0.5\sin\omega t$[bar]) (c) Mode 3 $(P'_f = 1 - 1\sin\omega t$[bar])

Figure 8. Outlines of P'_e and P'_f in each mode.

where the air pressure value is always positive, and then, $-P'_{f0} \leq A_f \leq P'_{f0}$. From Equations (16) and (22) and $(\hat{X}, \hat{V})$, P'_e can be calculated.

Figure 8 shows examples of calculated P'_e and P'_f when parameters in Table 1, $\hat{X}_0 = 0.8$ m, $\hat{A} = 0.02$ m and $T = 3$ s were used. With mode 1, P'_f and P'_e were in-phase, that is, agonist and antagonist muscles co-contracted (Figure 8(a)). In this case, the joint stiffness around these muscles became large, and then, the movement of the robot became stiff. Whereas, P'_f and P'_e were anti-phase, that is, agonist and antagonist muscles contracted alternately when mode 2 was used (Figure 8(b)). In this case, the joint stiffness around these muscles became small. When mode 3 was used, P'_e and P'_f are also in-phase (Figure 8(c)). However, smaller pressure inputs than mode 1 also could achieve the same motion. Moreover, P'_e and P'_f are anti-phase with the reference trajectory. In this case, agonist and antagonist muscles were extracted simultaneously when the hip position moved upward. The situation is beyond our expectation and quite interesting.

Above these results suggest that various movement can be realized using P'_e and P'_f and the redundancy of inputs will be able to use to a design of a desired joint stiffness. In the following section, we propose a design procedure of inputs based on a reference period trajectory and the desired joint stiffness.

Table 1. Parameters in Equation (22).

Mode	P'_{f0} bar	A_f bar	Phase difference between P'_e and P'_f
Mode 1	1	1	In-phase
Mode 2	1	−0.5	Anti-phase
Mode 3	1	−1	In-phase

4.2. Definition of joint stiffness

We define the joint stiffness of the robot model as

$$\begin{aligned} k &= -\frac{\partial F}{\partial X} = -ma_2 \\ &= -\frac{\partial}{\partial X}\Big(G_e(X) f_e(P'_e, L_e(X), v_e(X, V)) \\ &\quad - G_f(X) f_f(P'_f, L_f(X), v_f(X, V)) \Big). \end{aligned} \tag{23}$$

The k represents the variation of ground reaction force F with respect to the change of X. It should be noted that the joint stiffness k is strongly related to a_2. In other words, a_2 can be regarded as an index of joint stiffness as discussed in [7].

Figure 9 shows the estimated joint stiffness k with $P'_{f0} = 0.4\,\text{bar}$, $\hat{X}_0 = 0.8\,\text{m}$, $\hat{A} = 0.02\,\text{m}$ and $T = 3\,\text{s}$. Figure 9(a) and (b) shows the relationship between t, A_f and k and a projection of the relationship onto the t-k plane, respectively. It can be seen that (1) the value of k becomes large around a local maximum of X ($t \approx 0.8\,\text{s}$) and small around a local minimum ($t \approx 2.3\,\text{s}$) in all cases and (2) k considerably changes around local maximum and minimum points depending on A_f. We also verified that the increase in P'_{f0} increased the overall value of k. From these results, it can verified that the pattern of the inputs design can modify the joint stiffness k.

4.3. Design of pressure inputs based on a reference periodic motion and joint stiffness

Until this section, k was calculated using the following procedure (Figure 10(a)): (1) determine P'_f from Equation (22), (2) calculate P'_e using P'_f and reference trajectory $(\hat{X}, \hat{V})$ from Equation (16), and (3) calculate k using P'_f, P'_e and $(\hat{X}, \hat{V})$ from Equation (23). Although the transition of k depending on A_f and P'_{f0} was verified, an available design of k is still restricted only by the findings. Then, we modify the procedure.

Because P'_e can be expressed as a function of P'_f and $(\hat{X}, \hat{V})$, Equation (23), which is the function of P'_e, P'_f, $\hat{X}$ and $\hat{V}$, can be rewritten as a function of $\hat{X}$, $\hat{V}$ and P'_f with Equation (16), that is,

$$\begin{aligned} \hat{k} &= -\frac{\partial}{\partial X}\Big(G_e(\hat{X}) f_e(P'_e(\hat{X}, \hat{V}, P'_f), L_e(\hat{X}), v_e(\hat{X}, \hat{V})) \\ &\quad - G_f(\hat{X}) f_f(P'_f, L_f(\hat{X}), v_f(\hat{X}, \hat{V})) \Big) \end{aligned} \tag{24}$$

$$= -\frac{\partial}{\partial X}\Big(G_e(\hat{X}) \bar{f}_e(P'_f, \hat{X}, \hat{V}) - G_f(\hat{X}) \bar{f}_f(P'_f, \hat{X}, \hat{V}) \Big) \tag{25}$$

Using this relation, P'_f can be calculated from $(\hat{X}, \hat{V})$ and $\hat{k}$ numerically. Then, the modified design procedure of inputs is summarized as follows (Figure 10(b)); (1) calculate P'_f using $(\hat{X}, \hat{V})$ and $\hat{k}$ from Equation (25), and (2) calculate P'_e using calculated P'_f and $(\hat{X}, \hat{V})$ from Equation (16). Using this procedure, the design of pressure inputs based on the reference motion and joint stiffness can be achieved.

Here, it should be noted that an arbitrary value of $\hat{k}$ cannot be used. $\hat{k}$ should be feasible, that is, the calculated P'_f and P'_e values from $\hat{X}$, $\hat{V}$ and $\hat{k}$ have to satisfy some constants. P'_f and P'_e should always be positive. Practically, these values have an upper limit depends on the performance of the compressor and regulator. $\hat{k}$ should be designed according to a desired behavior of the robot in the first place. Therefore, in this study, we just verify that it is possible to design P'_f and P'_e based on $\hat{X}$, $\hat{V}$ and $\hat{k}$; a detailed consideration about the design of $\hat{k}$ will be studied in a future work.

As a simple example, we designed two pattern of $\hat{k}$ based on Figure 9. The first one $\hat{k}_{\max}$ consists of an upper limit of plotted data in Figure 9(b) and the second $\hat{k}_{\min}$ consist of a lower limit. The designed $\hat{k}_{\max}$ and $\hat{k}_{\min}$ values are shown in Figure 11. From the design method, $\hat{k}_{\max}$ or $\hat{k}_{\min}$ are always expected to largest or smallest. Figure 12 shows the calculated P'_f and P'_e values based on $\hat{k}_{\max}$ and $\hat{k}_{\min}$. For convenience, the reference trajectory $\hat{X}$ is also plotted.

4.4. Experiment results

We confirmed the validity of the designed inputs P'_f and P'_e through experiments with the developed robot. The experimental setup was the same as described in Section 3.3. Figure 13 shows the experimental results with P'_f and P'_e in Figure 12. It can be seen that the robot showed stable periodic motion and the desired trajectory was approximately achieved in both case when using $k_{\max}$ and $k_{\min}$ although there were some tracking errors. Here, there is a difference in the tracking performance of the two parameters $k_{\max}$ and $k_{\min}$. In the case of $k_{\max}$, the desired trajectory was achieved at all times, whereas the tracking error increases before and after the hip position is at its lowest in the case of $k_{\min}$. Before

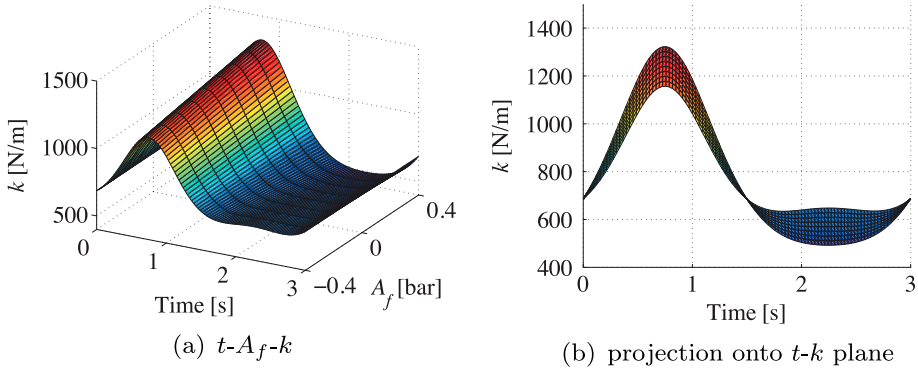

Figure 9. Estimated joint stiffness k.

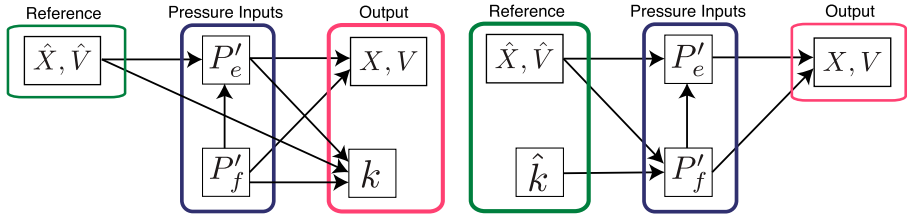

(a) $\hat{P}'_e$ is calculated based on $\hat{P}'_f$, $\hat{X}$ and $\hat{V}$. k is calculated based on $\hat{P}'_f$, $\hat{P}'_e$, $\hat{X}$ and $\hat{V}$.

(b) $\hat{P}'_f$, $\hat{P}'_e$ are calculated based on $\hat{X}$, $\hat{V}$ and $\hat{k}$

Figure 10. Design of pressure inputs based on a reference periodic motion and joint stiffness.

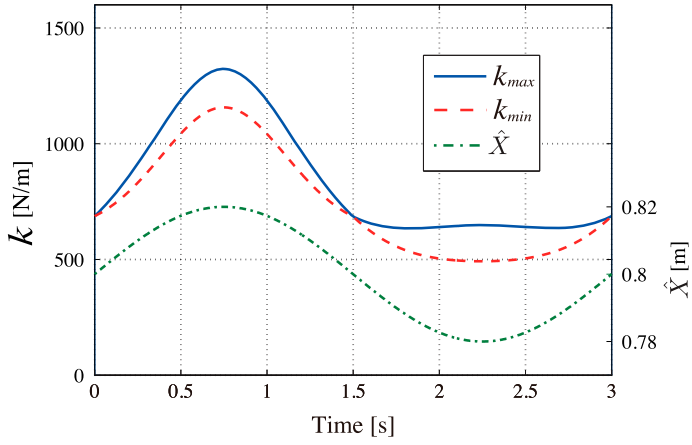

Figure 11. Designed k_{max} and k_{min} based on Figure 9(b).

and after the hip position is at its lowest, the large force is necessary to prevent a falling down to the ground. Because of this reason, it seems that the difference in joint stiffness k tends to appear more readily before and after the hip position is at its lowest. We conducted another experiment to verify that responses to disturbance are different depending on joint stiffness. As an example of disturbance, we added an additional 1 kg load at the hip and repeated the experiment with the same P'_f and P'_e values. Figure 14 shows the experimental results. In this case, although the both case show the periodic motion, the difference in the tracking performance of $k_{\max}$ and $k_{\min}$ is more clear.

From these results, it can be verified that the calculated P'_f and P'_e values based on $\hat{X}$, $\hat{V}$ and $\hat{k}$ could produce the desired periodic trajectory and the behavior of the robot could be regulated by changing $\hat{k}$.

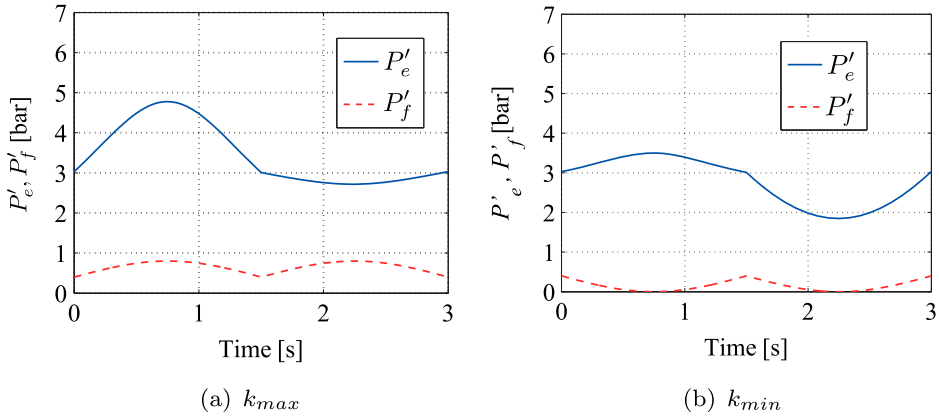

Figure 12. Calculated P'_f and P'_e based on $k_{\max}$ and $k_{\min}$.

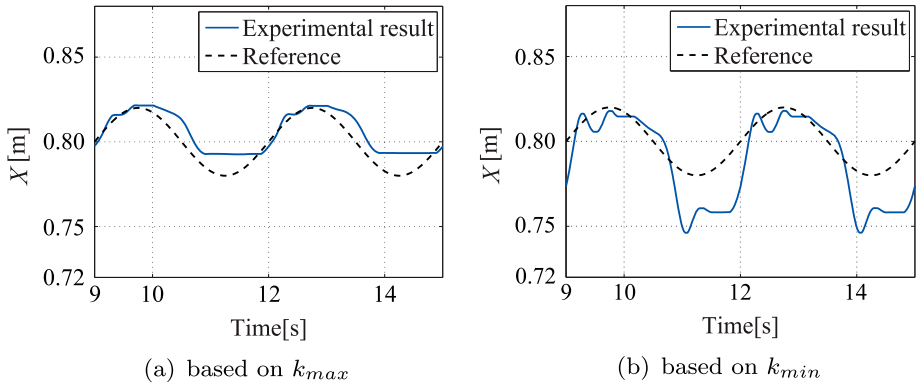

Figure 13. Experimental results with two calculated inputs.

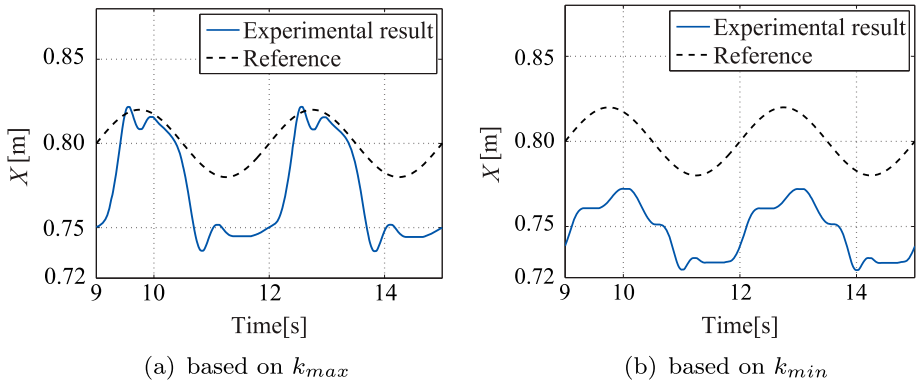

Figure 14. Experimental results under 1 kg static load.

5. Conclusion

In this study, which focuses on the periodic motion of a robot driven by an MPA, we introduced the stability criterion for periodic motion similar to our previous work [22], and showed that the criterion was always satisfied and the analysis strongly depended on the force-contraction velocity property of the MPA. Next, we focused on the redundancy of air pressure inputs. As one of application of the redundancy, we investigated the joint stiffness of the robot and proposed the design procedure of inputs based on the reference period trajectory and the desired joint stiffness. The stability analysis and design of joint stiffness were verified not only through numerical simulations but also through experiments with a developed 1-DOF legged robot.

Other applications of the redundancy of inputs, a detailed consideration of the joint stiffness, and the establishment of an analytical joint stiffness design will be studied in a future work. And the stability analysis of this paper is based on the linearity of the viscosity of MPA

in Equation (4) or the property $\frac{df}{dv} < 0$ (Equation (3)). Other types of actuators may have these properties. The application of this result for other types of actuators is also the future work.

Disclosure statement

No potential conflict of interest was reported by the authors.

Funding

This research was supported by CREST, JST and JSPS KAKENHI, Grant-in-Aid for JSPS Fellows [A268220].

Notes on contributors

Yasuhiro Sugimoto received the PhD degree from Kyoto University, Japan. From 2005 to 2008, he was an assistant professor at Kyoto University. In 2009, he became an assistant professor in the Department of Mechanical Engineering, Osaka University, Japan, where he became a lecturer in 2014 and he is currently an associate professor in 2016. His research interests include walking robots, artificial muscle and bio-inspired robotics. He is a member of the RSJ, SICE, JSME.

Daisuke Nakanishi received his BS and MS degrees from Osaka University, Japan, in 2012 and 2014 respectively. He is currently a doctor course student in the Department of Mechanical Engineering, Osaka University, Japan. His research interests include artificial muscles and mechatronics. He is a member of JSME and Japan Fluid Power System Society.

Motoki Nakanishi received his BS degrees from Osaka University, Japan, in 2014. He is currently a master course student in the Department of Mechanical Engineering, Osaka University, Japan. His research interests include artificial muscles and mechatronics.

Koichi Osuka graduated from the master's course of Graduate School of Engineering Science, Osaka University in March, 1984. Afterwards, he joined TOSHIBA, and worked for R&D Center. From 1986, he was in Univ. of Osaka Prefecture. From 1998, he had been an associate professor of Kyoto University. From 2003, he had been a professor of Kobe University. From 2009, he has been a professor of Osaka University. His research interests include control engineering and robotics. He is a member of The Philosophical Association of Japan, SICE, IEEE, RSJ and JSME. He received Dr.Eng. in 1989.

References

[1] Collins S, Ruina A, Tedrake R, et al. Efficient bipedal robots based on passive dynamic walkers. Sci Mag. 2005;307(5712):1082–1085.

[2] Wisse M, van der Linde R. Delft pneumatic bipeds. Vol. 34, Springer tracts in advanced robotics, Berlin: Springer; 2007.

[3] Takuma T, Hosoda K. Controlling the walking period of a pneumatic muscle walker. Int J Rob Res. 2006;25(9):861–866.

[4] Niiyama R, Nagakubo A, Kuniyoshi Y. Mowgli: a bipedal jumping and landing robot with an artificial musculoskeletal system. In: Proceedings of IEEE International Conference on Robotics and Automation; Roma, Italy; 2007. p. 2546–2551.

[5] Hosoda K, Takuma T, Nakamoto A, et al. Biped robot design powered by antagonistic pneumatic actuators for multi-modal locomotion. Rob Auton Syst. 2008;56(1):46–53.

[6] Sugimoto Y, Naniwa K, Osuka K, et al. Static and dynamic properties of McKibben pneumatic actuator for self-stability of legged-robot motion. Adv Rob. 2013;27(6):469–480.

[7] Nakanishi D, Sueoka Y, Sugimoto Y, et al. Investigation for the stability of standing posture and stiffness of robot driven by mckibben pneumatic actuator. In: Proceedings of 2014 International Symposium on Flexible Automation (ISFA2014); Hyogo, Japan; 2014. p. 2014–103S.

[8] Verrelst B, Daerden F, Lefeber D, et al. Introducing pleated pneumatic artificial muscles for the actuation of legged robots: a one-dimensional setup. In: Proceedings of International Conference on Walking and Climbing Robots (CLAWAR 2000); Madrid, Spain; 2000. p. 583–590.

[9] Shimizu M, Suzuki K, Narioka K, et al. Roll motion control by stretch reflex in a continuously jumping musculoskeletal biped robot. In: IEEE/RSJ International Conference on Intelligent Robots and Systems; Vilamoura, Portugal; 2012. p. 1264–1269.

[10] Niiyama R, Nishikawa S, Kuniyoshi Y. Biomechanical approach to open-loop bipedal running with a musculoskeletal athlete robot. Adv Rob. 2012;26(3–4):383–398.

[11] Narioka K, Rosendo A, Sproewitz A, et al. Development of a minimalistic pneumatic quadruped robot for fast locomotion. In: IEEE International Conference on Robotics and Biomimetics (ROBIO 2012); Guangzhou, China; 2012. p. 307–311.

[12] van der Linde RQ. Design, analysis, and control of a low power joint for walking robots, by phasic activation of McKibben muscles. IEEE Trans Rob Autom. 1999;15(4):599–604.

[13] Verrelst B, Van Ham R, Vanderborght B, et al. The pneumatic biped 'LUCY' actuated with pleated pneumatic artificial muscles. Auton Rob. 2005;18(2):201–213.

[14] Sugisaka M, Zhao H. The characteristics of McKibben muscle based on the pneumatic experiment system. Artif Life Rob. 2007;11(2):223–226.

[15] Takuma T, Hayashi S, Hosoda K. 3D bipedal robot with tunable leg compliance mechanism for multi-modal locomotion. In: IEEE/RSJ International Conference on Intelligent Robots and Systems; Nice, France; 2008. p. 1097–1102.

[16] Tondu B, Lopez P. Modeling and control of McKibben artificial muscle robot actuators. IEEE Control Syst Mag. 2000;20(2):15–38.

[17] Chou CP, Hannaford B. Measurement and modeling of McKibben pneumatic artificial muscles. IEEE Trans Rob Autom. 1996;12(1):90–102.
[18] Klute GK, Hannaford B. Accounting for elastic energy storage in McKibben artificial muscle actuators. J Dyn Syst Meas Control. 2000;122(2):386–388.
[19] Klute GK, Czerniecki JM, Hannaford B. Artificial muscles: actuators for biorobotic systems. Int J Rob Res. 2002;21(4):295–309.
[20] Reynolds DB, Repperger DW, Phillips CA, et al. Modeling the dynamic characteristics of pneumatic muscle. Ann Biomed Eng. 2003;31(3):310–317.
[21] Doumit M, Fahim A, Munro M. Analytical modeling and experimental validation of the braided pneumatic muscle. IEEE Trans Rob. 2009;25(6):1282–1291.
[22] Sugimoto Y, Aoi S, Ogihara N, et al. Stabilizing function of the musculoskeletal system for periodic motion. Adv Rob. 2009;23(5):521–534.

Appendix: Symbols, definition and values in MPA and robot model

The detailed MPA model we used in this paper is:

$$\begin{aligned} f(P', L, v) &= -P' \frac{\mathrm{d}V_b}{\mathrm{d}L} + V_r \frac{\mathrm{d}W}{\mathrm{d}L} - f_v(v) \\ &= -P' \frac{\mathrm{d}V_b}{\mathrm{d}L} \\ &\quad + V_r \Bigg[C_1 \left\{ \frac{2L}{L_0^2} - \frac{2L}{D_0^2 n^2 \pi^2} \right. \\ &\quad \left. - \frac{2L_0^2 D_0^2 n^2 \pi^2 (b^2 - 2L^2)}{L^3 (b^2 - L^2)^2} \right\} \\ &\quad + C_2 \left\{ -\frac{2L_0^2}{L^3} + \frac{2D_0^2 n^2 \pi^2 L}{(b^2 - L^2)^2} + \frac{2Lb^2 - 4L^3}{L_0^2 D_0^2 n^2 \pi^2} \right\} \Bigg] - \gamma v. \end{aligned} \tag{1}$$

Parameters of the MPA model and robot model are listed in Tables A1 and A2.

Table A1. Symbols, definition and values in MPA model.

Symbols	Definitions	Values
L	Length of MPA	–
v	Contractile velocity of MPA	–
P'	Relative pressure between an absolute internal air pressure and environment pressure	–
C_1	Mooney-Rivlin constant	192 kPa
C_2	Mooney-Rivlin constant	1.3 kPa
D_0	Actuator's resting state diameter	15 mm
b	Braid length	148 mm
n	Number of turns	1.68
γ	Viscosity coefficient of actuator model	30 Ns/m
L_0	Resting state length of MPA	–

Table A2. Symbols, definition and values in the robot model.

Symbols	Definitions	Values
L_o	Length from knee to hip (Length of femur)	450 mm
L_u	Length of lower link (Length of tibia)	425 mm
L_1	Length from knee to flexor (inside) actuator attached position of upper link	200 mm
L_2	Length from knee to flexor (inside) actuator attached position of lower link	100 mm
r	Radius of knee pulley	40 mm
m	Representative mass of leg and hip	3.74 kg
g	Gravitational acceleration	9.86 $\mathrm{m/s^2}$
F	Ground reaction force	–
X	Vertical displacement of hip	–
V	Velocity of the location of the hip	–
β	Angle of knee	–
f_e, f_f	Extensor (outside)/flexor (inside) MPA force	–
G_e, G_f	Geometric transformation of extensor/flexor MPA	–
L_e, L_f	Length of extensor/flexor MPA	–
P'_e, P'_f	Pressure of extensor/flexor MPA	–
v_e, v_f	Contractile velocity of extensor/flexor MPA	–
L_{e0}, L_{f0}	Resting state length of extensor/flexor	125 mm
l_{Mf}	Length of flexor MPA + Length of wire	–